Temperature converges, precipitation diverges: a systematic evaluation of three Quaternary paleoclimate reconstructions over the last 800,000 years

Alexander Gamisch[1]

[1]Independent Researcher, 5020 Salzburg, Austria

Corresponding author

Name: Alexander Gamisch

Address: 5020 Salzburg, Austria

E-Mail: alexandergamisch@gmx.at

ORCID: https://orcid.org/0000-0002-9698-4344

Short running head: **Temperature converges, precipitation diverges**

Number of text pages: 41

Number of Figures: 6

Number of Tables: 3

Word count: 5480

Supplementary Material: This article contains supplementary material.

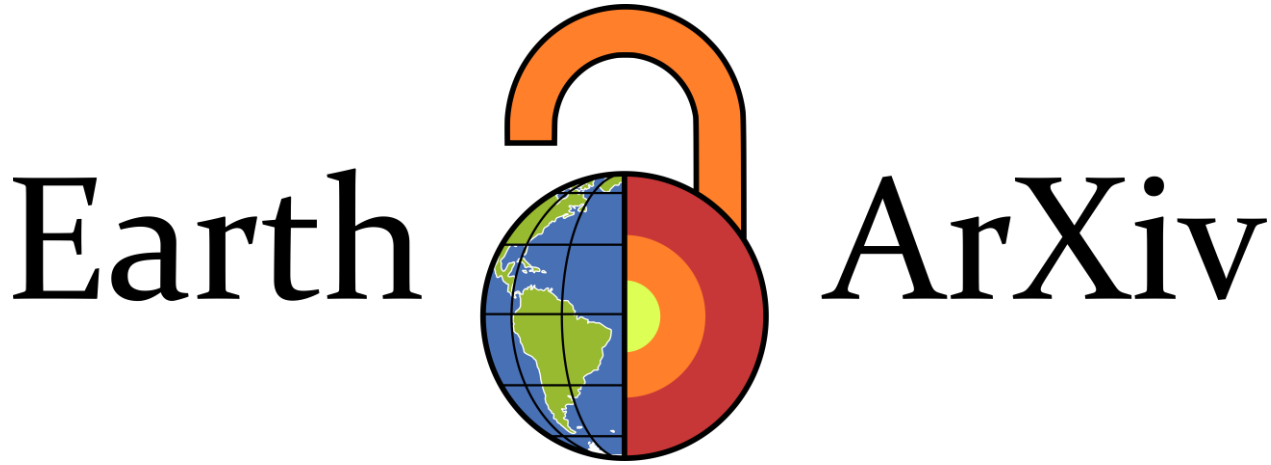

Abstract

Aim

Spatially explicit paleoclimate reconstructions are widely used in macroecology, biogeography, and archaeology to infer past species ranges, refugia, and biodiversity dynamics. Three products, Oscillayers, Krapp et al. (2021), and PALEO-PGEM-Series, provide global bioclimatic variables across the Quaternary, yet rest on fundamentally different methodological foundations, and their mutual consistency remains unquantified.

Methods

This study provides the first joint comparison of all three reconstructions on a common bioclimatic grid across 79 time slices spanning 20–800 ka BP, focusing on mean annual temperature (BIO1) and total annual precipitation (BIO12). Agreement was assessed via raw-value and anomaly correlations, partial correlations controlling for latitude, root mean squared error, threshold-based agreement rates, and validation against 19 independent terrestrial proxy archives, including the first continuous time-series validation of Oscillayers. Inter-dataset consistency rather than absolute accuracy is quantified; proxy archives serve as the single external benchmark.

Main conclusions

The results reveal a clear contrast between variables. For temperature, all dataset pairs showed high spatial correlations ($r = 0.98–0.99$) and consistently positive cell-wise temporal correlations across virtually the entire terrestrial realm, with disagreement concentrated in high-latitude regions (northern North America, Siberia). For precipitation, spatial patterns remained correlated ($r = 0.94–0.95$), but anomaly correlations were near zero ($r = 0.05–0.19$), with large areas of negative temporal correlation across the Amazon Basin, Congo Basin, and South and Southeast Asia. Proxy validation yielded comparable performance across all three datasets (mean $|r| \approx 0.50$). The three reconstructions are largely interchangeable for studies centred on broad-scale temperature gradients, but should not be treated as equivalent for analyses requiring past precipitation histories, particularly in tropical and monsoonal regions. Dataset choice should be treated as explicit uncertainty rather than an arbitrary background decision.

Keywords: Quaternary paleoclimate, bioclimatic reconstructions, dataset comparison, macroecology, Oscillayers, precipitation uncertainty, species distribution modelling

Introduction

Across macroecology, biogeography, and archaeology, spatially explicit reconstructions of paleoclimate have become indispensable inputs for investigating past species ranges, biodiversity dynamics, and human prehistory (Willmes et al. 2020; Lawing 2021; Blois et al. 2025; Licht et al. 2026; Lomborg et al. 2026). Such reconstructions are used to identify (glacial) refugia, reconstruct the range dynamics of taxa from plants to hominins, quantify long-term niche evolution, and trace the climatic contexts of major biogeographic transitions (e.g. Kougioumoutzis et al. 2020; Beyer et al. 2021; Bergman et al. 2023; Folk et al. 2023; Lu et al. 2023; Timmermann et al. 2024; Gamboa et al. 2024; Schweickl et al. 2025; Jongsma et al. 2026). Yet the paleoclimatic datasets underpinning these inferences were built from fundamentally different assumptions, forcing data, and modelling frameworks and their agreement across space and time has not been systematically quantified.

Among the currently available long-term reconstructions (summarized in Barreto et al. 2023; Lomborg et al. 2026), three products now provide spatially explicit bioclimatic variables at a global scale across the Quaternary: Oscillayers (Gamisch 2019), the reconstruction of Krapp et al. (2021), and PALEO-PGEM-Series (Holden et al. 2019; Barreto et al. 2023). All three span at least the last 800 kyr and provide the bioclimatic variables routinely used in species distribution and niche modelling, yet they rest on fundamentally different methodological foundations (Table 1). Oscillayers is generated by statistically scaling present-to-LGM climate anomalies along a global temperature curve derived from benthic oxygen-isotope ratios (Hansen et al. 2013; Gamisch 2019), an approach that assumes the spatial structure of climate anomalies to remain constant through time, with only its amplitude varying in proportion to the global temperature curve. Krapp et al. (2021) instead derive transient climatologies from linear regressions between snapshots of the HadCM3 general circulation model and external forcings (atmospheric CO_2, orbital parameters, and surface type), bias-corrected against present-day observations. PALEO-PGEM-Series takes a third approach, statistically emulating PLASIM-GENIE, an intermediate-complexity atmosphere–ocean model that captures coupled climate dynamics at lower computational cost than a fully coupled GCM, before downscaling the emulated fields to a modern climatological baseline. These frameworks thus span a gradient from purely statistical rescaling to the

emulation of a coupled climate model, and each rests on simplifying assumptions whose consequences for the reconstructed bioclimatic variables remain incompletely understood (Gamisch 2019, 2020; Brown et al. 2020; Krapp et al. 2021; Barreto et al. 2023).

Whether these methodological differences translate into meaningful disagreement in the reconstructed bioclimatic fields, and if so, where and when, is an open question with direct practical consequences. Paleoclimatic reconstructions do not enter ecological and archaeological analyses as raw climate fields: they are transformed into estimates of habitat suitability, connectivity, and niche overlap, and used to infer the timing and geography of range shifts, refugial persistence, and dispersal events. If inter-product disagreements are systematic, concentrated in particular regions, time periods, or climatic states, then studies relying on a single reconstruction may carry unacknowledged sensitivity to dataset choice (Varela et al. 2015; Rentier et al. 2025; Guevara et al. 2025), with potentially different inferences about the location of climatically suitable areas, the degree of population connectivity, or the persistence of glacial refugia (e.g. Kirschner et al. 2020; Guevara et al. 2025).

Despite the growing reliance on these long-term reconstructions, systematic cross-dataset evaluation remains incomplete. First, Oscillayers has been assessed against bioclimatic snapshots at individual time slices (Gamisch 2019, 2020; Brown et al. 2020), but has not been validated against independent terrestrial archives in a continuous time-series framework. Second, PALEO-PGEM and the Krapp et al. reconstruction have each been evaluated against proxy records (Barreto et al. 2023; Krapp et al. 2021, their Table 4), but their mutual agreement at the level of gridded bioclimatic variables has not been quantified. Third, all three reconstructions have never been jointly compared on a common bioclimatic grid across their shared temporal range. In addition, concerns have been raised about the stationarity assumption underlying Oscillayers, that the spatial structure of climate anomalies remains invariant through time (Gamisch 2019, 2020; Brown et al. 2020; Barreto et al. 2023), leading to the expectation that Oscillayers may reconstruct systematically different bioclimatic conditions than the model-based products. Whether this is the case, and if so where and when it manifests, has not yet been empirically established. Critically, these evaluations have so far quantified inter-product *consistency* rather than absolute accuracy; the same framework is adopted here, treating proxy archives as the single external benchmark against which consistency can be partially evaluated.

This study addresses these gaps by comparing Oscillayers, PALEO-PGEM-Series, and the reconstruction of Krapp et al. across 79 time slices at 10 kyr resolution spanning 20–800 ka BP, using mean annual temperature (BIO1) and total annual precipitation (BIO12). Reconstruction agreement was quantified using four complementary approaches: (i) similarity in absolute climate patterns, assessed through Pearson correlation, partial correlation controlling for latitude, mean bias, and root mean squared error (RMSE); (ii) agreement in temporal climate anomalies relative to each dataset's long-term mean; (iii) the proportion of the terrestrial land surface for which climate estimates converged within ecologically meaningful uncertainty thresholds; and (iv) the ability of each reconstruction to reproduce temperature variability recorded in 19 independent terrestrial proxy archives spanning up to 800 kyr BP, including the first time-series validation of Oscillayers. The first three analyses were conducted both for individual time slices and on a cell-wise basis across the full temporal record, enabling assessment of both the temporal and spatial dimensions of reconstruction agreement. Collectively, these analyses provide a quantitative framework for evaluating the conditions under which paleoclimatic reconstructions are interchangeable, that is, whether substituting one product for another is likely to alter the qualitative conclusions of a downstream ecological or biogeographic analysis, and for identifying regions and time periods where dataset choice warrants explicit sensitivity testing.

Materials and Methods

Data sources

Three independent global paleoclimate reconstructions (i.e. Oscillayers (Gamisch 2019); HadCM3 climate simulations extended via linear regression (Krapp et al. 2021; hereafter Krapp); PALEO-PGEM-Series (Holden et al. 2019; Barreto et al. 2023; hereafter PGEM)) were compared across 79 time steps spanning the last 800 thousand years (kyr) (Table 1). Oscillayers provides bioclimatic reconstructions for the past 5.4 million years at a spatial resolution of 0.04° × 0.04° and a temporal resolution of 10 kyr (Gamisch 2019). In contrast, Krapp covers the last 800 kyr at 1 kyr intervals and a spatial resolution of 0.5° × 0.5°, whereas PGEM offers bioclimatic reconstructions spanning the past 5 million years at 1 kyr intervals and a spatial resolution of 1° × 1°. The three paleoclimate datasets were

downloaded from their respective repositories (Oscillayers: https://doi.org/10.5061/dryad.27f8s90, Krapp: https://doi.org/10.17605/OSF.IO/8N43X; PGEM: https://figshare.com/s/d45714f7212de7225fe2. All analyses focused on mean annual temperature (BIO1, °C) and total annual precipitation (BIO12, mm yr^{-1}).

Data processing

To facilitate comparisons among palaeoclimatic datasets differing in spatial and temporal resolution and extent, all analyses were conducted on a common 10 kyr time grid and a 0.5° × 0.5° spatial grid and common paleo-coastlines for each time step. The temporal resolution (10 kyr) was chosen to match Oscillayers, whereas the spatial resolution followed the 0.5° × 0.5° reference grid of Krapp et al. (2021). The temporal window of 20–800 ka BP was determined by the coverage of Oscillayers, which provides no reconstructions for time steps more recent than 20 ka. The upper bound of 800 ka BP was chosen to encompass the full shared temporal range of all three products. Oscillayers and PGEM were resampled to this grid using bilinear interpolation. To ensure consistency in land–sea distribution through time, the Krapp and PGEM datasets were subsequently masked using the corresponding Oscillayers land mask for each of the 79 time steps. For each dataset, the long-term mean climate at each grid cell was calculated as the arithmetic mean across all 79 time slices spanning 20–800 ka BP. Temporal anomalies were subsequently derived by subtracting this cell-specific mean from the reconstructed value at each time slice. Consequently, anomaly values represent the signed departure of climatic conditions from the long-term mean at a given grid cell and time step. To characterise agreement at two complementary analytical levels, pairwise metrics were computed both across space for each time step and across time for each grid cell. The time-step-level metrics, describing how spatial agreement varies over time, are presented first, followed by cell-wise metrics aggregated over all 79 time steps, which yield spatially explicit maps of where agreement is consistently high or low. Together, these two levels address when and where the reconstructions converge.

Time-step-level inter-dataset comparison

For each of the three comparison pairs, Oscillayers–Krapp, PGEM–Krapp, and Oscillayers–PGEM, and each time step, the following metrics were computed: Pearson absolute correlation (r_{abs}); anomaly correlation (r_{anom}); latitude-partial correlation (r_{part}); mean bias (data set 1, DS1 − data set 2, DS2); RMSE. Agreement percentages (%) were computed at four thresholds per variable (BIO1: ±1, 1.5, 3, 5 °C; BIO12: ±50, 100, 200, 300 mm). Agreement percentages were compared against LGM inter-model agreement values from Gamisch (2020) as a contextual reference. This benchmark reflects agreement between two GCMs at a single time slice and therefore represents a conservative lower bound rather than a direct methodological equivalent to the present multi-temporal, multi-framework comparison. For each pairwise comparison at each time step, only cells with simultaneously non-missing values for the absolute values of both datasets, their respective temporal anomalies, and latitude were retained. Sequences of all 79 time steps for both variables are provided in the Supplement (Additional File 1, Additional File 2) and at the Dryad digital repository [doi: https://doi.org/10.5061/dryad.qrfj6q5z8] to allow visual inspection of how spatial agreement evolves through the glacial–interglacial cycles.

Cell-wise spatial analysis

For each grid cell, the temporal Pearson (r_{ts}) correlation between two datasets' 79-step value time series was computed. High positive r_{ts} indicates that both datasets reconstruct similar temporal trajectories at a given location; negative values indicate anti-phase temporal dynamics. For each cell, the mean bias was computed as the arithmetic mean of (DS1 − DS2) across all 79 time steps, and the mean RMSE as the square root of the mean squared difference. Temporal agreement percentages (%) were computed at four thresholds per variable (BIO1: ±1, 1.5, 3, 5 °C; BIO12: ±50, 100, 200, 300 mm). These cell-wise aggregates reveal whether systematic or random disagreements are spatially uniform or concentrated in particular regions.

Proxy validation

To evaluate temporal correspondence between the three reconstructions and geological temperature archives, BIO1 was validated against 19 terrestrial paleoclimate proxy records, following the methodology of Krapp et al. (2021) and Barreto et al. (2023). Site metadata and time series were obtained from Krapp et al. (2021) (DOI: 10.17605/OSF.IO/8N43X) (see Supplement Table S1). Each proxy time series was linearly interpolated to the 10 kyr grid and the temporal overlap between each proxy and each dataset was determined and rounded inward to the nearest 10 ka step. For each proxy site and dataset, BIO1 was extracted from the nearest grid cell at native spatial resolution, and Pearson r and p-values were computed over all valid overlapping time steps. Published Pearson r values from Krapp et al. (2021) and Barreto et al. (2023) (computed over the full 800 ka record at 19 terrestrial sites at steps of 1 kyr) were used as a reference benchmark.

Software

All analyses were conducted in R v. 4.5.3 (R Core Team 2026) using the functionalities of the following packages: “terra” v. 1.9-27 (Hijmans et al. 2026), “ncdf4” v. 1.24 (Pierce 2025), “readxl” v. 1.4.5 (Wickham & Bryan 2025), “ggplot2” v. 4.0.3 (Wickham 2016), “dplyr” v. 1.2.1 (Wickham, François, et al. 2026), “tidyr” v. 1.3.2 (Wickham, Vaughan, et al. 2025), ”cowplot” v. 1.2.0 (Wilke 2025), “patchwork” v. 1.3.2 (Pedersen 2025), “scales” v. 1.4.0 (Wickham, Pedersen, et al. 2025), and “sf” v. 1.1.1 (Pebesma 2018; Pebesma & Bivand 2023). Code available at the Dryad digital repository [doi: https://doi.org/10.5061/dryad.qrfj6q5z8].

Results

Comparison of the three paleoclimate reconstructions across 79 time slices (20–800 ka BP) revealed a clear contrast between temperature (BIO1) and precipitation (BIO12) (Fig. 1). This contrast is illustrated for a single representative glacial time step (20 ka BP) in Figures 2 (BIO1) and 3 (BIO12), and quantified across the full record in the cell-wise summaries (Figs. 4, 5) and threshold analyses (Fig. 6) described below. For BIO1, all dataset pairs showed very high absolute spatial correlations (r_{abs} =

0.983–0.991; Table 2; Fig. 1a), indicating a consistent representation of global temperature gradients. Agreement in temporal anomalies was lower and temporally variable (mean r_{anom} = 0.441–0.555; Table 2, Fig. 1b), with negative values at isolated time steps in all pairs, most pronounced for Oscillayers–PGEM (e.g. −0.762 at 230 ka BP; 14/79 steps negative) and PGEM–Krapp (−0.735 at 390 ka BP; 13/79 steps negative). Despite this temporal variability, cell-wise temporal correlations (r_{ts}) for BIO1 were highly positive across virtually the entire terrestrial realm for all three dataset pairs (Fig. 4a), indicating that the long-term directional temperature signal is consistently reproduced across space. Mean RMSE values for BIO1 were lowest for Oscillayers–Krapp (3.37 °C) and Oscillayers–PGEM (3.41 °C), and highest for PGEM–Krapp (4.19 °C), consistent with these bias patterns (Table 2, Fig. 1c). Oscillayers and PGEM were systematically warmer than Krapp (mean biases +1.76 °C and +2.15 °C, respectively) (Table 2, Fig. 1d), with spatial disagreement concentrated in high-latitude continental regions, particularly northern North America and Siberia, where cell-wise mean RMSE values locally exceeded the ≥9 °C colour bar limit (Fig. 4a). At 20 ka BP (Fig. 2), a representative glacial time step, all three reconstructions reproduced a closely concordant global temperature structure (r_{abs} = 0.979–0.991; Fig. 2e), confirming that the high mean spatial agreement is already expressed at the level of an individual time slice. Consistent with the multi-step results, the residual disagreement was spatially structured rather than random, concentrated over the formerly glaciated and periglacial regions of northern North America, Greenland, and northern Eurasia (Fig. 2c), while tropical and subtropical temperatures were reconstructed almost identically across products. Partial correlations, computed after removing the linear latitudinal effect, remained consistently high for both variables and all pairs (BIO1: mean $r_{partial}$ = 0.972, 0.952, 0.953; BIO12: mean $r_{partial}$ = 0.922, 0.939, 0.921 for Oscillayers–Krapp, Oscillayers–PGEM, and PGEM–Krapp, respectively), differing negligibly from the corresponding absolute correlations (mean $|r_{abs} - r_{partial}| \leq 0.03$ in all cases), confirming that the high spatial agreement reflects structural congruence rather than a latitudinal gradient artefact (Table 2, see Supplement Table S2).

In contrast, BIO12 showed substantially weaker agreement in temporal variability. Although absolute spatial precipitation patterns remained highly correlated (r_{abs} = 0.937–0.950, Fig. 1e), anomaly correlations were near zero (r_{anom} = 0.051–0.193; Fig. 1f), indicating that the three products reconstruct largely independent precipitation histories through time (Table 2). The near-zero r_{anom} for Oscillayers–

PGEM (0.051) was not the result of cancellation between regions of positive and negative correlation, but reflected genuine spatial incoherence, with large contiguous areas of negative cell-wise temporal correlation (r_{ts}) across South and Southeast Asia, sub-Saharan Africa, and South America (Fig. 4b). Mean RMSE for BIO12 ranged from 223 mm (Oscillayers–PGEM) to 252 mm (PGEM–Krapp) (Table 2, Fig. 1g), with highest values concentrated in tropical regions, particularly the Amazon Basin, the Congo Basin, and Southeast Asia (Fig. 4b). The contrast with precipitation is already evident at this single glacial time step (Fig. 3). Although the broad geography of wet and dry regions was reproduced consistently (r_{abs} = 0.905–0.920; Fig. 3e), the pairwise difference maps revealed extensive and spatially incoherent disagreement throughout the humid tropics, most pronounced across Amazonia, the Congo Basin, and South and Southeast Asia (Fig. 3c), with anomaly correlations close to zero (r_{anom} = 0.084–0.229; Fig. 3e). Thus, even at the Last Glacial Maximum, the most intensively studied interval of the Quaternary, the three reconstructions disagree substantially on regional precipitation. Both Oscillayers and PGEM exhibited positive precipitation biases relative to Krapp (+16.9 mm and +21.6 mm, respectively; Table 2, Fig. 1h). Across the 800 ka record, cell-wise agreement rates were lowest in humid tropical and monsoonal regions, the Amazon Basin, tropical Africa, and South and Southeast Asia, whereas arid regions showed consistently high agreement (Fig. 4b).

A closer examination of ecologically relevant thresholds reveals a more nuanced picture of inter-dataset concordance (Fig. 5). For BIO1, the Oscillayers–PGEM pair achieved cell-wise mean agreement rates across all timepoints of 50.3% at ±1.5 °C (Table 3), exceeding the contextual lower bound LGM benchmark of 40.7% (Gamisch 2020) for 68/79 (c.86%) of time points (see Supplement Table S2, Table 3, Fig. 5a). Oscillayers–Krapp also exceeded the benchmark at this threshold (mean 44.9% across all timepoints) for 45/79 (c.56%) of time points, while PGEM–Krapp fell below it (mean 35.9% across all timepoints) for 26/79 (c.32%) of time points, identifying the latter as the most divergent pair at fine temperature thresholds (see Supplement Table S2). For BIO12, mean agreement rates at ±100 mm reached 64.7% (Oscillayers–PGEM), 62.1% (Oscillayers–Krapp), and 55.6% (PGEM–Krapp), indicating that across roughly half to two thirds of the global land surface absolute precipitation differences remained within this range on average. This threshold was exceeded in more than 50% of grid cells at nearly all time steps (≥74 of 79 time slices for all pairs), suggesting that the moderate global

mean agreement is not driven by a small number of outlier time steps but reflects a consistent pattern across the 800 ka record (Table 3, Fig. 5b).

Across both variables and particularly for temperature and for absolute-pattern and RMSE-based metrics, Oscillayers consistently occupied the central position in the comparison triangle, agreeing better with each of the other two datasets than they agree with each other. Overall, the three reconstructions provide a largely consistent representation of temperature variability over the last 800 kyr, whereas precipitation reconstructions diverge substantially, particularly in tropical and monsoon-dominated regions.

Proxy validation

All three datasets showed comparable proxy validation performance across 19 terrestrial sites (mean $|r| \approx 0.50$; Fig.6; see Supplemental Figure S1, see Supplement Table S3), closely matching both the Krapp et al. (2021) reference mean of 0.489 and the reference values reported by Barreto et al. (2023; mean $|r| = 0.511$; median $|r| = 0.600$; 13/19 sites with $|r| \geq 0.5$). The sign of the proxy–temperature relationship was reproduced at 19/19 sites by Oscillayers and Krapp, and at 18/19 by PGEM. Strongest and most consistent agreement was found at Mediterranean speleothem sites (Peqiin: $|r| \approx 0.80$; Soreq: $|r| \approx 0.78$) and Chinese loess–palaeosol sequences (Xifeng, Chanwu, Yimaguan Luochuan: $|r| = 0.58$–0.67). The largest inter-dataset spread in $|r|$ occurred at Dead Sea (range 0.262), Clearwater (0.254), and Lake El'gygytgyn (0.250), identifying regions where dataset choice materially affects proxy-based temperature reconstruction. Uniformly low agreement at Sanbao-Dongge ($|r| \leq 0.10$) and Lake Baikal ($|r| \leq 0.22$) across all three datasets is consistent with published reference values and reflects the limited sensitivity of these proxies to annual mean temperature.

Discussion

This study provides the first joint, spatially and temporally explicit comparison of three widely used global paleoclimate reconstructions, Oscillayers, Krapp et al. (2021), and PALEO-PGEM-Series, across their shared 800 kyr record on a common bioclimatic grid. The results reveal a clear and

consistent asymmetry between variables. Despite spanning a methodological gradient from statistical rescaling of present-to-LGM anomalies to regression-based GCM extrapolation and coupled-model emulation, all three products provide a broadly coherent representation of mean annual temperature structure across the terrestrial realm. Precipitation histories, by contrast, diverge substantially, particularly in their temporal evolution in humid tropical and monsoon-dominated regions. The proxy validation indicates that all three products capture major terrestrial temperature signals to a comparable degree, including Oscillayers, for which this study provides the first continuous time-series validation against independent terrestrial archives. Together, these findings suggest that long-term paleoclimate reconstructions are more interchangeable for questions centred on broad-scale thermal gradients than for questions requiring past hydrological dynamics.

The high correspondence among temperature fields supports the view that the dominant thermal architecture of the Quaternary climate system is consistently captured regardless of the underlying methodological approach, a pattern also documented in previous multi-dataset comparisons of paleoclimate reconstructions (Varela et al. 2015; Fordham et al. 2017; Folk et al. 2023). Much of the spatial variation in mean annual temperature is governed by large-scale energy-balance constraints, including latitude, elevation, continentality and the distribution of ice sheets. The persistence of high partial correlations after accounting for latitude indicates that this agreement is not attributable to the shared latitudinal thermal gradient alone, but extends to major regional contrasts among continents, mountain systems and high-latitude landmasses. This consistency should not, however, be equated with accuracy. The three reconstructions are not fully independent: they share present-day climatological baselines and are anchored, directly or indirectly, to global benthic oxygen-isotope signal (Gamisch 2019; Krapp et al. 2021; Barreto et al. 2023), so part of their mutual agreement might reflect shared inputs rather than independent convergence on past temperature. With this caveat, the result remains important for macroecology and biogeography, because many applications of paleoclimate layers rely on the broad spatial arrangement of thermal environments to infer potential ranges, climatic connectivity or niche evolution (Lawing et al. 2016; Rodriguez et al. 2021; Hosfield 2022; Folk et al. 2023). For such applications, the three datasets convey a broadly coherent signal.

At the same time, the lower and temporally variable anomaly correlations show that agreement in raw spatial patterns does not imply agreement in the timing or magnitude of local departures from long-term mean conditions. This distinction is consequential for studies of Quaternary range dynamics, in which species distribution models, demographic reconstructions, and phylogeographic inferences depend not only on whether a region is broadly warm or cold, but on whether it becomes relatively more or less suitable during particular glacial or interglacial intervals (Guevara et al. 2025). The strong cell-wise temporal correlations for temperature indicate that the long-term directionality of temperature change is broadly conserved across space, so that temperature-based inferences about glacial refugial persistence, climatic stability, or repeated exposure to cooling are likely to be relatively robust across reconstructions. The isolated negative anomaly correlations at individual time steps, most pronounced for Oscillayers–PGEM at 230 ka BP ($r_{anom} = -0.76$) and for PGEM–Krapp at 390 ka BP ($r_{anom} = -0.74$), most plausibly reflect minor chronological offsets in the placement of glacial–interglacial extrema rather than genuine climatic disagreement among reconstructions; visual inspection of the animated time-step sequences (Additional File 1) supports this interpretation, showing that periods of low spatial anomaly correlation typically coincide with rapid transitions (spikes) rather than with stable climatic states. This interpretation is consistent with the high cell-wise temporal correlations observed at these same locations and provides a concrete mechanistic basis for treating inferences tied to single 10 kyr slices with greater caution than those based on long-term trajectories.

The concentration of temperature disagreement in high-latitude continental regions is consistent with known challenges in reconstructing Quaternary climates (Varela et al. 2015; Kageyama et al. 2021). Northern North America and Siberia experienced major changes in ice-sheet extent, albedo, sea level, vegetation cover and atmospheric circulation (Kageyama et al. 2021). These factors introduce strong nonlinearities that are difficult to capture consistently across statistical and model-based approaches, and relatively small differences in how reconstructions represent ice volume, surface type or the translation of global temperature curves into regional anomalies can generate large differences in mean annual temperature.

Notably, this spatial pattern of temperature disagreement mirrors findings from fully coupled climate model ensembles: in both PMIP3 and PMIP4, inter-model spread in mean annual temperature is largest

precisely in the northern extratropics and over formerly glaciated regions, even as global mean cooling is reproduced consistently (Kageyama et al. 2021). This suggests that high-latitude temperature uncertainty is an inherent challenge of palaeoclimate reconstruction, not an artefact of the particular methodological approaches compared here. From a biogeographic perspective, these areas are also among the most consequential for reconstructing glacial refugia, postglacial colonization routes and high-latitude extinction dynamics. The observed spatial structure of disagreement therefore provides a practical guide: paleobiogeographic studies in formerly glaciated or periglacial regions should explicitly evaluate the sensitivity of conclusions to the choice of paleoclimate product, especially when thermal thresholds are ecologically meaningful (Varela et al. 2015; Rentier et al. 2025).

A more specific question motivating this comparison was whether the stationarity assumption underlying Oscillayers imposes a systematic disadvantage relative to the more physically explicit reconstructions (Brown et al. 2020; Gamisch, 2020; Barreto et al. 2023). For temperature, and for absolute-pattern and RMSE-based metrics, no such disadvantage was detected: Oscillayers agreed at least as closely with each model-based product as those products agreed with one another across the last 800 kyr. This result should nonetheless be read cautiously rather than as an endorsement: mutual agreement among partly dependent products is not a measure of accuracy, and the available proxy archives lack the power to discriminate among the three reconstructions. The appropriate conclusion is not that any product is superior but that the relevant question is one of fitness for purpose rather than of overall quality.

The precipitation results reveal a more complex picture. Absolute precipitation patterns are still strongly correlated among datasets, indicating that the reconstructions agree on the broad geography of wet and dry regions. This is encouraging for analyses that depend mainly on large-scale aridity gradients, such as distinguishing deserts, savannas, temperate regions and humid tropical forests. However, the near-zero anomaly correlations and extensive areas of negative cell-wise temporal correlation show that the temporal evolution of annual precipitation differs substantially among datasets. This pattern reflects a fundamental and well-documented property of paleoclimate modelling rather than a limitation specific to the products compared here. Analysing nine fully coupled GCMs for the Last Glacial Maximum, Varela et al. (2015) found that temperature variables (BIO1–BIO11) are highly correlated between

models, whereas precipitation variables (BIO12–BIO19) show consistently low inter-model correlations, with tropical regions displaying the greatest disagreement, a pattern they attribute to the nonlinear sensitivity of convective and monsoonal systems to orbital forcing, ice-sheet geometry and regional feedbacks. Our results extend this finding across the full 800 kyr record and across reconstructions that differ not only in their GCM heritage but in their fundamental methodological approach, providing the first systematic quantification of this asymmetry over the long Quaternary and establishing a baseline against which future improvements in paleo-precipitation reconstruction can be assessed. Part of this divergence is likely also inherited from the modern climatological baselines on which the reconstructions are anchored: WorldClim (Hijmans et al. 2005) and CHELSA (Karger et al. 2017), the two primary baselines used across the three products, themselves disagree substantially for annual precipitation, with approximately 60% of global land cells differing by more than ±25 mm under present-day conditions alone (Gamisch 2020). Because these baseline differences are largest in the humid tropics and monsoon regions (Gamisch 2020), they are likely to amplify rather than merely add to the methodological divergence introduced by the paleo-scaling procedures. This caveat applies most directly to the Oscillayers–PGEM pair, which are built on WorldClim and CHELSA respectively; the Krapp et al. (2021) product, bias-corrected against observational data, introduces a third baseline framework, further compounding the sources of inter-product precipitation disagreement. Strikingly, within the PMIP4 ensemble alone, where all models share the same ice-sheet configuration, greenhouse gas concentrations and boundary conditions, individual simulations (i.e. 9 out 13 models) still disagree on the sign of LGM precipitation change across large areas of the tropics and monsoon domains (Kageyama et al. 2021, their Fig. 6). This intra-ensemble divergence under identical forcing demonstrates that tropical precipitation uncertainty is not primarily a function of differing boundary conditions or methodological choices, but reflects the chaotic and nonlinear sensitivity of atmospheric circulation to glacial forcing, a sensitivity that is expected to be at least as pronounced, if not greater, in reconstructions spanning 800 kyr of varying orbital and ice-volume configurations. This conclusion is reinforced by Kageyama et al. (2021), who show that even between successive generations of coupled climate models (PMIP3 vs. PMIP4), precipitation changes, particularly in the tropics, remain the most

heterogeneous and least reproducible component of LGM simulations, with large inter-model differences persisting despite substantial improvements in model physics.

The strongest hydrological disagreement, concentrated in the Amazon Basin, Congo Basin, and South and Southeast Asia, is especially relevant for ecology and evolution. These regions contain the world's highest species richness and have been central to debates about rainforest stability, refugial fragmentation, biome shifts, and diversification under Quaternary climate change (Gamisch & Comes, 2019; Schweickl et al. 2025). If reconstructions differ in whether tropical regions became wetter or drier during particular intervals, then models of past habitat suitability, biome turnover, or population connectivity may diverge accordingly, with contrasting implications for speciation, extinction, and the spatial accumulation of endemism (Blois et al. 2025; Schweickl et al. 2025; Guevara et al. 2025). The apparently high agreement in arid regions deserves a parallel caveat: because annual precipitation is low in deserts and semi-arid systems, absolute difference thresholds are easier to satisfy, and high agreement rates within ±100 mm may partly reflect the small magnitude of precipitation rather than close correspondence in hydrological dynamics. These findings reinforce the case for multi-dataset approaches in studies of tropical and monsoonal palaeoenvironments (Varela et al. 2015; Rentier et al. 2025; Guevara et al. 2025).

The proxy validation provides an independent perspective on reconstruction performance. Broadly comparable mean absolute correlations across all three datasets (mean $|r| \approx 0.50$) indicate that no reconstruction is consistently superior across terrestrial temperature archives, shifting the interpretation from a simple ranking toward a context-dependent view of utility. Strongest and most consistent agreement was found at Mediterranean speleothem sites and Chinese loess–palaeosol sequences, where proxy systems are sensitive to mean annual temperature or closely related dimensions; uniformly weak agreement at Sanbao-Dongge and Lake Baikal likely reflects proxy-specific sensitivities, these archives record a mixture of temperature, precipitation, seasonality, and source effects, rather than reconstruction failure alone (Beyer et al. 2021; Krapp et al. 2021; Barreto et al. 2023). Comparisons were conducted at each dataset's native spatial resolution, giving Oscillayers a theoretical advantage for point-level extraction at topographically heterogeneous sites. That this finer resolution does not translate into consistently higher proxy correlations is consistent with the hypothesis that temporal fidelity, rather

than spatial precision, is the primary determinant of proxy–model agreement at these timescales, though spatial mismatch, chronological uncertainty, and proxy seasonality effects cannot be fully excluded as confounding factors.

Framed as a question of fitness for purpose, several practical implications follow for macroecology, biogeography and evolutionary biology. First, studies focused on thermal niche conservatism, broad-scale range shifts, climatic exposure or continental-scale refugial dynamics may rest on a relatively solid basis when using any of the three reconstructions, provided that uncertainty in high-latitude regions is acknowledged. Second, studies focused on precipitation-driven biome dynamics, tropical forest stability, monsoon variability or hydrological corridors should avoid reliance on a single paleoclimate product. Third, and most generally, the results argue for treating paleoclimate reconstructions not as interchangeable background layers but as alternative hypotheses about past environmental conditions (Varela et al. 2015; Rentier et al. 2025); comparing biological conclusions across reconstructions helps distinguish robust signals from dataset-dependent artefacts (Guevara et al. 2025).

Several limitations should be acknowledged. Most fundamentally, the analyses quantify mutual consistency rather than accuracy: because the reconstructions share baselines and forcing signals, agreement may overstate genuine reliability. Resampling to a common 0.5° grid was necessary for comparability but smooths fine-scale climatic heterogeneity in topographically complex regions. The focus on BIO1 and BIO12 cannot capture the full climatic niche space relevant to organisms; temperature seasonality, drought indices, and moisture availability may show different agreement patterns. The proxy validation is limited to terrestrial temperature archives and provides no equivalent assessment of precipitation. Spatial and temporal autocorrelation in gridded climate fields and proxy series reduce effective degrees of freedom, so the correlation-based metrics are best interpreted as descriptive rather than as formal significance tests. Finally, agreement thresholds are necessarily general, since climatic tolerances vary widely across taxa, life stages, and ecological contexts.

In conclusion, the three paleoclimate reconstructions examined here are broadly interchangeable, in the sense that substituting one for another is unlikely to alter the qualitative conclusions of a downstream

analysis, for studies centred on broad-scale temperature gradients, long-term thermal trajectories, or continental-scale refugial dynamics, provided that uncertainty in high-latitude regions is acknowledged. For studies centred on precipitation-driven biome dynamics, tropical forest stability, monsoon variability, or hydrological corridors, the reconstructions should not be treated as equivalent, and biological conclusions that depend on past precipitation histories should be explicitly evaluated across multiple products. More generally, the results support treating paleoclimate reconstructions not as unconditionally interchangeable background layers but as alternative hypotheses about past environmental conditions, comparing conclusions across reconstructions to distinguish robust signals from dataset-dependent artefacts (Varela et al. 2015; Rentier et al. 2025; Guevara et al. 2025). Recognizing this temperature–precipitation asymmetry allows paleoclimate data to be used more effectively: with confidence where reconstructions converge and are corroborated by proxies, with caution where they diverge, and with explicit uncertainty where biological conclusions depend on climatic histories that remain difficult to reconstruct.

References

Barreto, E., Holden, P. B., Edwards, N. R., & Rangel, T. F. (2023). PALEO-PGEM-Series: A spatial time series of the global climate over the last 5 million years (Plio-Pleistocene). *Global Ecology and Biogeography*, *32*, 1034–1045.

Bergman, J., Pedersen, R. Ø., Lundgren, E. J., Lemoine, R. T., Monsarrat, S., Pearce, E. A., … Svenning, J. C. (2023). Worldwide Late Pleistocene and Early Holocene population declines in extant megafauna are associated with *Homo sapiens* expansion rather than climate change. *Nature Communications*, *14*, 7679.

Beyer, R. M., Krapp, M., Eriksson, A., & Manica, A. (2021). Climatic windows for human migration out of Africa in the past 300,000 years. *Nature Communications*, *12*, 4889.

Blois, J. L., Bellvé, A. M., Jarzyna, M. A., Saupe, E. E., & Syverson, V. J. (2025). Paleobiogeographic insights gained from ecological niche models: Progress and continued challenges. *Paleobiology*, *51*, 8–28.

Brown, J. L., Hill, D. J., & Haywood, A. M. (2020). A critical evaluation of the Oscillayers methods and datasets. *Global Ecology and Biogeography*, *29*, 1435–1442.

Folk, R. A., Gaynor, M. L., Engle-Wrye, N. J., O'Meara, B. C., Soltis, P. S., Soltis, D. E., … Okuyama, Y. (2023). Identifying climatic drivers of hybridization with a new ancestral niche reconstruction method. *Systematic Biology*, *72*, 856–873.

Fordham, D. A., Saltré, F., Haythorne, S., Wigley, T. M., Otto-Bliesner, B. L., Chan, K. C., & Brook, B. W. (2017). PaleoView: A tool for generating continuous climate projections spanning the last 21,000 years at regional and global scales. *Ecography*, *40*, 1348–1358.

Gamboa, S., Galván, S., & Varela, S. (2024). Vrba was right: Historical climate fragmentation, and not current climate, explains mammal biogeography. *Global Change Biology*, *30*, e17339.

519 Gamisch, A. (2019). Oscillayers: A dataset for the study of climatic oscillations over Plio-Pleistocene
520 time-scales at high spatial-temporal resolution. *Global Ecology and Biogeography*, *28*, 1552–
521 1560.

522 Gamisch, A. (2020). A reply to the 'critical evaluation of the Oscillayers methods and dataset'. *Global*
523 *Ecology and Biogeography*, *29*, 1443–1448.

524 Gamisch, A., & Comes, H. P. (2019). Clade-age-dependent diversification under high species turnover
525 shapes species richness disparities among tropical rainforest lineages of *Bulbophyllum*
526 (Orchidaceae). *BMC Evolutionary Biology*, *19*, 93.

527 Guevara, L., Zugasti-Mateos, A., Pinilla-Buitrago, G. E., León-Tapia, M. Á., Vázquez-Domínguez, E.,
528 & Anderson, R. P. (2025). Which global circulation model works best for my region?
529 Concordance with genetic data for a Neotropical shrew. *Ecography*, *2025*, e07881.

530 Hansen, J., Sato, M., Russell, G., & Kharecha, P. (2013). Climate sensitivity, sea level and atmospheric
531 carbon dioxide. *Philosophical Transactions of the Royal Society A: Mathematical, Physical*
532 *and Engineering Sciences*, *371*, 20120294.

533 Hijmans, R. J., Cameron, S. E., Parra, J. L., Jones, P. G., & Jarvis, A. (2005). Very high resolution
534 interpolated climate surfaces for global land areas. *International Journal of Climatology*, *25*,
535 1965–1978.

536 Hijmans, R. J., Brown, A., & Barbosa, M. (2026). *terra*: Spatial data analysis (R package version 1.9-
537 27). Retrieved from https://CRAN.R-project.org/package=terra

538 Holden, P. B., Edwards, N. R., Rangel, T. F., Pereira, E. B., Tran, G. T., & Wilkinson, R. D. (2019).
539 PALEO-PGEM v1.0: A statistical emulator of Pliocene–Pleistocene climate. *Geoscientific*
540 *Model Development*, *12*, 5137–5155.

541 Hosfield, R. (2022). Variations by degrees: Western European paleoenvironmental fluctuations across
542 MIS 13–11. *Journal of Human Evolution*, *169*, 103213.

543 Jongsma, G. F., Barve, N., Allen, J. M., Owens, H. L., & Blackburn, D. C. (2026). Pleistocene forest
544 stability predicts patterns of frog diversity in Central Africa. *Ecology and Evolution*, *16*,
545 e73207.

546 Kageyama, M., Harrison, S. P., Kapsch, M. L., Löfverström, M., Lora, J. M., Mikolajewicz, U., …
547 Volodin, E. (2021). The PMIP4-CMIP6 Last Glacial Maximum experiments: Preliminary
548 results and comparison with the PMIP3-CMIP5 simulations. *Climate of the Past*, *17*, 1–37.

549 Karger, D. N., Conrad, O., Böhner, J., Kawohl, T., Kreft, H., Soria-Auza, R. W., … Kessler, M. (2017).
550 Climatologies at high resolution for the earth's land surface areas. *Scientific Data*, *4*, 1–20.

551 Kirschner, P., Záveská, E., Gamisch, A., Hilpold, A., Trucchi, E., Paun, O., … Schoenswetter, P.
552 (2020). Long-term isolation of European steppe outposts boosts the biome's conservation value.
553 *Nature Communications*, *11*, 1968.

554 Kougioumoutzis, K., Kokkoris, I. P., Panitsa, M., Trigas, P., Strid, A., & Dimopoulos, P. (2020). Plant
555 diversity patterns and conservation implications under climate-change scenarios in the
556 Mediterranean: The case of Crete (Aegean, Greece). *Diversity*, *12*, 270.

557 Krapp, M., Beyer, R. M., Edmundson, S. L., Valdes, P. J., & Manica, A. (2021). A statistics-based
558 reconstruction of high-resolution global terrestrial climate for the last 800,000 years. *Scientific*
559 *Data*, *8*, 228.

560 Lawing, A. M. (2021). The geography of phylogenetic paleoecology: Integrating data and methods to
561 better understand biotic response to climate change. *Paleobiology*, *47*, 178–197.

562 Lawing, A. M., Polly, P. D., Hews, D. K., & Martins, E. P. (2016). Including fossils in phylogenetic
563 climate reconstructions: A deep time perspective on the climatic niche evolution and
564 diversification of spiny lizards (*Sceloporus*). *The American Naturalist*, *188*, 133–148.

565 Licht, A., Sanmartín, I., Meseguer, A. S., Boschman, L., Vaes, B., Quintero, I., … Beard, K. C. (2026).
566 Integrating Earth history into phylogenetic diversification models. *Trends in Ecology &*
567 *Evolution*.

Lomborg, K. L., Cucart-Mora, C., Reschke, J. O., Hertler, C., Grove, M., Gaudou, B., … Moncel, M. H. (2026). Changing movements in a changing world: Modelling Early Pleistocene and Early Middle Pleistocene climatic and ecological environments and influences on hominin dispersal in Eurasia. *Journal of Computer Applications in Archaeology*, *9*, 66–88.

Lu, W. X., Wang, Z. Z., Hu, X. Y., & Rao, G. Y. (2023). Echoes of the past: Niche evolution, range dynamics, and their coupling shape the distribution of species in the *Chrysanthemum zawadskii* species complex. *Frontiers in Ecology and Evolution*, *11*, 1250491.

Pebesma, E. (2018). Simple features for R: Standardized support for spatial vector data. *The R Journal*, *10*, 439–446.

Pebesma, E., & Bivand, R. (2023). *Spatial data science: With applications in R*. Boca Raton, FL: Chapman and Hall/CRC.

Pedersen, T. L. (2025). *patchwork*: The composer of plots (R package version 1.3.2). Retrieved from https://CRAN.R-project.org/package=patchwork

Pierce, D. (2025). *ncdf4*: Interface to Unidata netCDF (version 4 or earlier) format data files (R package version 1.24). Retrieved from https://CRAN.R-project.org/package=ncdf4

R Core Team. (2026). *R: A language and environment for statistical computing*. Vienna, Austria: R Foundation for Statistical Computing. Retrieved from https://www.R-project.org/

Rentier, E. S., Mottl, O., Pacheco-Riaño, L. C., Schultz, L., Seguinot, J., Wiersma, A. T., … Flantua, S. G. (2025). Global variability in LGM cooling amongst paleoclimate datasets affects biome reconstructions in mountains. *Frontiers of Biogeography*, *18*, e135871.

Rodriguez, J., Willmes, C., & Mateos, A. (2021). Shivering in the Pleistocene. Human adaptations to cold exposure in Western Europe from MIS 14 to MIS 11. *Journal of Human Evolution*, *153*, 102966.

Schweickl, K., Affenzeller, M., Nardi, F. D., Krenn, G., Fischer, G. A., & Comes, H. P. (2025). Temperature-dependent speciation in the Sundaland region driven by interglacial refugial

593 isolation in the *Bulbophyllum lobbii* complex (Orchidaceae). *Journal of Biogeography*, *52*,
594 e70102.

595 Timmermann, A., Raia, P., Mondanaro, A., Zollikofer, C. P., Ponce de León, M., Zeller, E., & Yun, K.
596 S. (2024). Past climate change effects on human evolution. *Nature Reviews Earth &*
597 *Environment*, *5*, 701–716.

598 Varela, S., Lima-Ribeiro, M. S., & Terribile, L. C. (2015). A short guide to the climatic variables of the
599 last glacial maximum for biogeographers. *PLOS ONE*, *10*, e0129037.

600 Wickham, H. (2016). *ggplot2: Elegant graphics for data analysis*. New York, NY: Springer-Verlag.

601 Wickham, H., & Bryan, J. (2025). *readxl*: Read Excel files (R package version 1.4.5). Retrieved from
602 https://CRAN.R-project.org/package=readxl

603 Wickham, H., François, R., Henry, L., Müller, K., & Vaughan, D. (2026). *dplyr*: A grammar of data
604 manipulation (R package version 1.2.1). Retrieved from https://CRAN.R-
605 project.org/package=dplyr

606 Wickham, H., Pedersen, T. L., & Seidel, D. (2025). *scales*: Scale functions for visualization (R package
607 version 1.4.0). Retrieved from https://CRAN.R-project.org/package=scales

608 Wickham, H., Vaughan, D., & Girlich, M. (2025). *tidyr*: Tidy messy data (R package version 1.3.2).
609 Retrieved from https://CRAN.R-project.org/package=tidyr

610 Wilke, C. O. (2025). *cowplot*: Streamlined plot theme and plot annotations for 'ggplot2' (R package
611 version 1.2.0). Retrieved from https://CRAN.R-project.org/package=cowplot

612 Willmes, C., Niedziółka, K., Serbe, B., Grimm, S. B., Groß, D., Miebach, A., … Bareth, G. (2020).
613 State of the art in paleoenvironment mapping for modeling applications in archeology—
614 Summary, conclusions, and future directions from the PaleoMaps Workshop. *Quaternary*, *3*,
615 13.

616

Data and Code Availability Statement

The data that supports the findings of this study are available in the supplementary material of this article and at the Dryad digital repository [doi: https://doi.org/10.5061/dryad.qrfj6q5z8].The data sets analysed in this study are openly available in (Dryad: https://doi.org/10.5061/dryad.27f8s90, Open Science Framework: https://doi.org/10.17605/OSF.IO/8N43X; figshare: https://figshare.com/s/d45714f7212de7225fe2.

Tables

Table 1. Overview of the three global paleoclimatic reconstructions compared in this study.

Feature	Oscillayers	Krapp et al. (2021)	PALEO-PGEM-Series
Methodological approach	Statistical scaling of interpolated present–LGM anomalies	Linear regression of GCM snapshots on external forcings	Statistical emulation of an intermediate-complexity AOGCM
Underlying climate source	Present-day and LGM (CCSM) climate layers	72 HadCM3 simulation snapshots	PLASIM-GENIE emulator
Scaling / forcing	Benthic $\delta^{18}O$ global temperature curve	CO_2, orbital parameters, surface type	CO_2, orbital parameters, ice volume
Bias correction / baseline	Present-day WorldClim	Present-day observations(CRU)	Modern CHELSA baseline
Temporal coverage	5.4 Myr (Plio-Pleistocene)	Last 800 kyr	≈5 Myr (Plio-Pleistocene)
Temporal resolution	10 kyr	1 kyr	1 kyr
Spatial resolution	0.04° × 0.04°	0.5° × 0.5°	1° × 1°
Variables	19 bioclimatic variables	Monthly/annual T, P, cloud cover; 17 bioclimatic variables	Monthly T, P, 17 bioclimatic variables

AOGCM, atmosphere–ocean general circulation model; CRU, Climatic Research Unit; GCM, general circulation model; LGM, Last Glacial Maximum; T, temperature; P, precipitation.

Table 2. Mean pairwise agreement metrics for annual mean temperature (BIO1) and total annual precipitation (BIO12), averaged across 79 time slices (20–800 ka BP). r_{abs}: Pearson correlation of raw values across all land grid cells; $r_{partial}$ (in parentheses): partial correlation after removing the linear latitudinal effect; r_{anom}: Pearson correlation of anomalies (deviations from the long-term temporal mean); Bias: mean difference DS1 − DS2; RMSE: root mean square error.

Bio1	**r_{abs} ($r_{partial}$)**	**r_{anom}**	**Bias (°C)**	**RMSE (°C)**
Oscillayers vs. Krapp	0.99 (0.97)	0.56	1.76	3.37
Oscillayers vs. PGEM	0.98 (0.95)	0.48	-0.38	3.41
PGEM vs. Krapp	0.98 (0.95)	0.44	2.15	4.19
Bio12	**r_{abs} ($r_{partial}$)**	**r_{anom}**	**Bias (mm)**	**RMSE (mm)**
Oscillayers vs. Krapp	0.94 (0.92)	0.15	16.93	249.13
Oscillayers vs. PGEM	0.95 (0.94)	0.05	-7.13	222.97
PGEM vs. Krapp	0.94 (0.92)	0.19	21.56	251.66

Table 3. Mean temporal agreement rates for annual mean temperature (BIO1) and total annual precipitation (BIO12), expressed as the percentage of grid cells within a specified absolute difference threshold, averaged over all 79 time slices (20–800 ka BP). Values represent the global mean of the cell-wise agreement rate (see Fig. 3) across the full temporal record. NA: no reference value available for this threshold in Gamisch (2020).

Bio1	**±1°C**	**±1.5°C**	**±3°C**	**±5°C**
Oscillayers vs. Krapp	31.08	44.90	73.22	88.19
Oscillayers vs. PGEM	36.70	50.33	73.58	87.42
PGEM vs. Krapp	24.22	35.85	62.17	80.28
MIROC vs. CCSM[1]	28.40	40.70	67.30	85.10
Bio12	**±50mm**	**±100mm**	**±200mm**	**±300mm**
Oscillayers vs. Krapp	39.78	62.13	82.43	90.14
Oscillayers vs. PGEM	43.05	64.74	83.57	90.47
PGEM vs. Krapp	34.55	55.57	77.72	86.92
MIROC vs. CCSM[1]	30.10	NA	67.10	78.20

[1]The MIROC vs. CCSM reference row (Gamisch 2020) is based on a single LGM time slice and two GCMs, and is included as a conservative contextual benchmark.

Figures

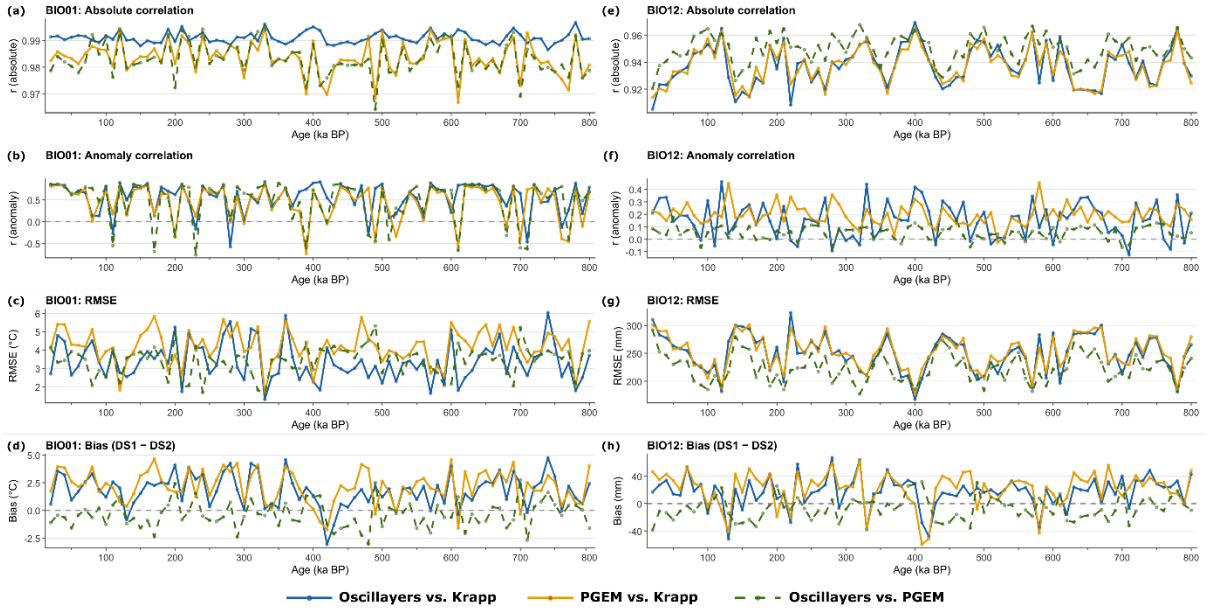

Figure 1. Time-step-level comparison of three paleoclimate reconstructions across 79 time slices (20–800 ka BP) for annual mean temperature (BIO1; panels a–d) and total annual precipitation (BIO12; panels e–h). Shown are pairwise absolute spatial correlation (r_{abs}; a, e), anomaly correlation (r_{anom}; b, f), root mean square error (RMSE; c, g), and mean bias (d, h) between Oscillayers vs. Krapp (blue, solid), PGEM vs. Krapp (orange, solid), and Oscillayers vs. PGEM (green, dashed). Each metric is computed across all land grid cells for each time step independently. Bias is defined as DS1 − DS2, where DS1 and DS2 correspond to the first and second dataset in each pair as listed in the legend. The dashed horizontal line in panels b, f, d, and h indicates zero.

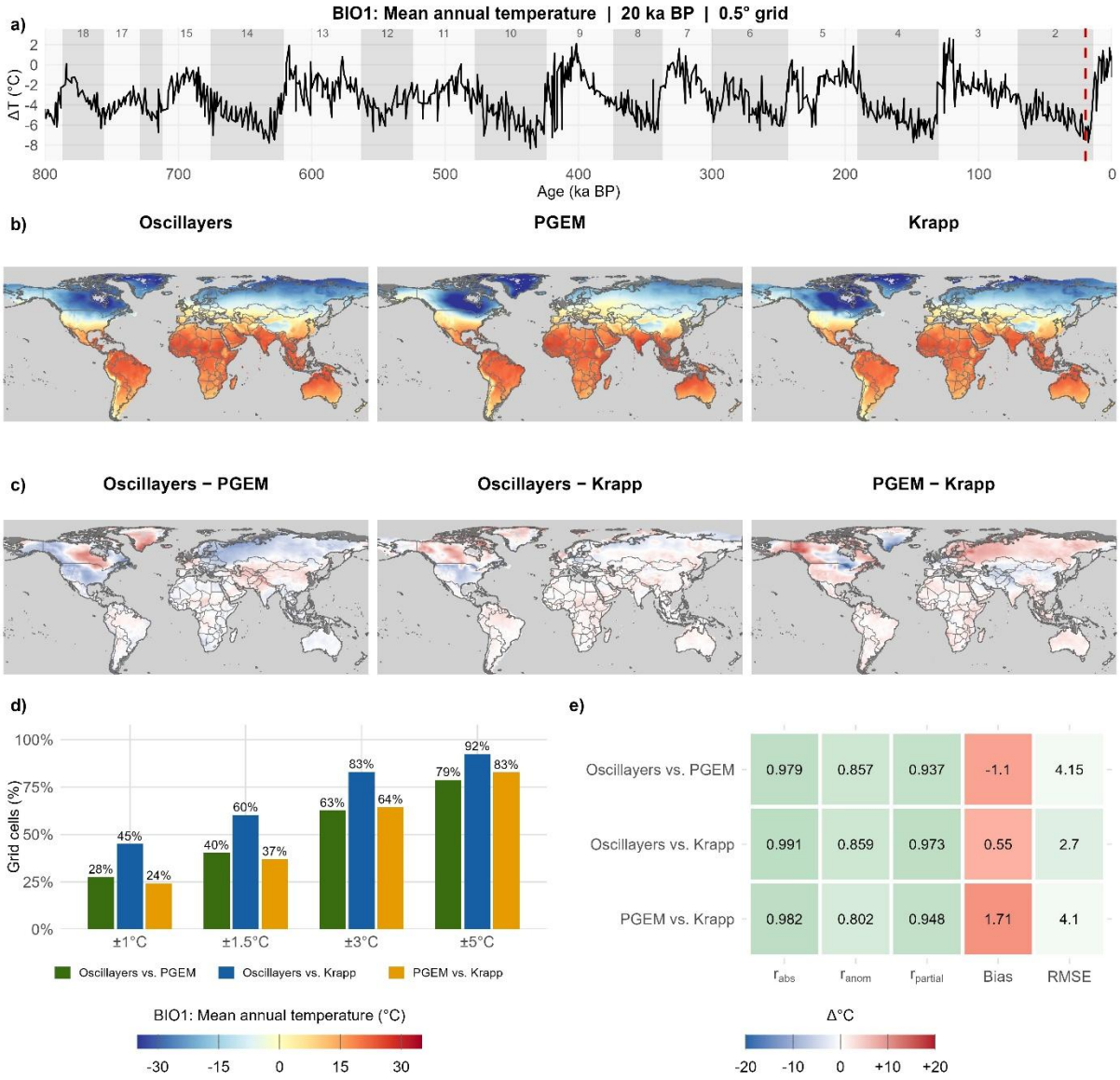

667

668 **Figure 2.** Comparison of mean annual temperature (BIO1) among the three paleoclimate
669 reconstructions, Oscillayers, PGEM, and Krapp, at a single representative glacial time step (20 ka BP),
670 on the common 0.5° grid using the Oscillayers land mask. (a) Global temperature anomaly curve of
671 Hansen et al. (2013) across the last 800 kyr, with alternating shaded bands denoting Marine Isotope
672 Stages (MIS 2–18, labelled); the red dashed line marks the time step shown. (b) Reconstructed BIO1
673 for each dataset. (c) Pairwise difference maps (Oscillayers − PGEM, Oscillayers − Krapp, PGEM −
674 Krapp); red indicates that the first dataset is warmer, blue that it is cooler. (d) Proportion of terrestrial
675 grid cells for which the two datasets of each pair agree within ±1, ±1.5, ±3, and ±5 °C. (e) Summary of
676 pairwise agreement metrics for this time step: raw-value spatial correlation (r_{abs}), anomaly correlation
677 ($_{ranom}$), latitude-partial correlation ($r_{partial}$), mean bias (°C), and RMSE (°C); cell shading indicates the

degree of agreement (green = stronger, red = weaker). Note that the metrics in (e) refer to this single time step and therefore differ from the multi-step means reported in the main text and Table 2; anomaly correlations at the Last Glacial Maximum are higher than the long-term average, reflecting the spatially coherent cooling signal of full glacial conditions. Residual disagreement is concentrated over formerly glaciated and periglacial regions of northern North America, Greenland, and northern Eurasia, while tropical and subtropical temperatures are reconstructed almost identically across products. Sequences of all 79 time steps are provided in the Supplement (Additional File 1; see also Dryad repository (doi: https://doi.org/10.5061/dryad.qrfj6q5z8)).

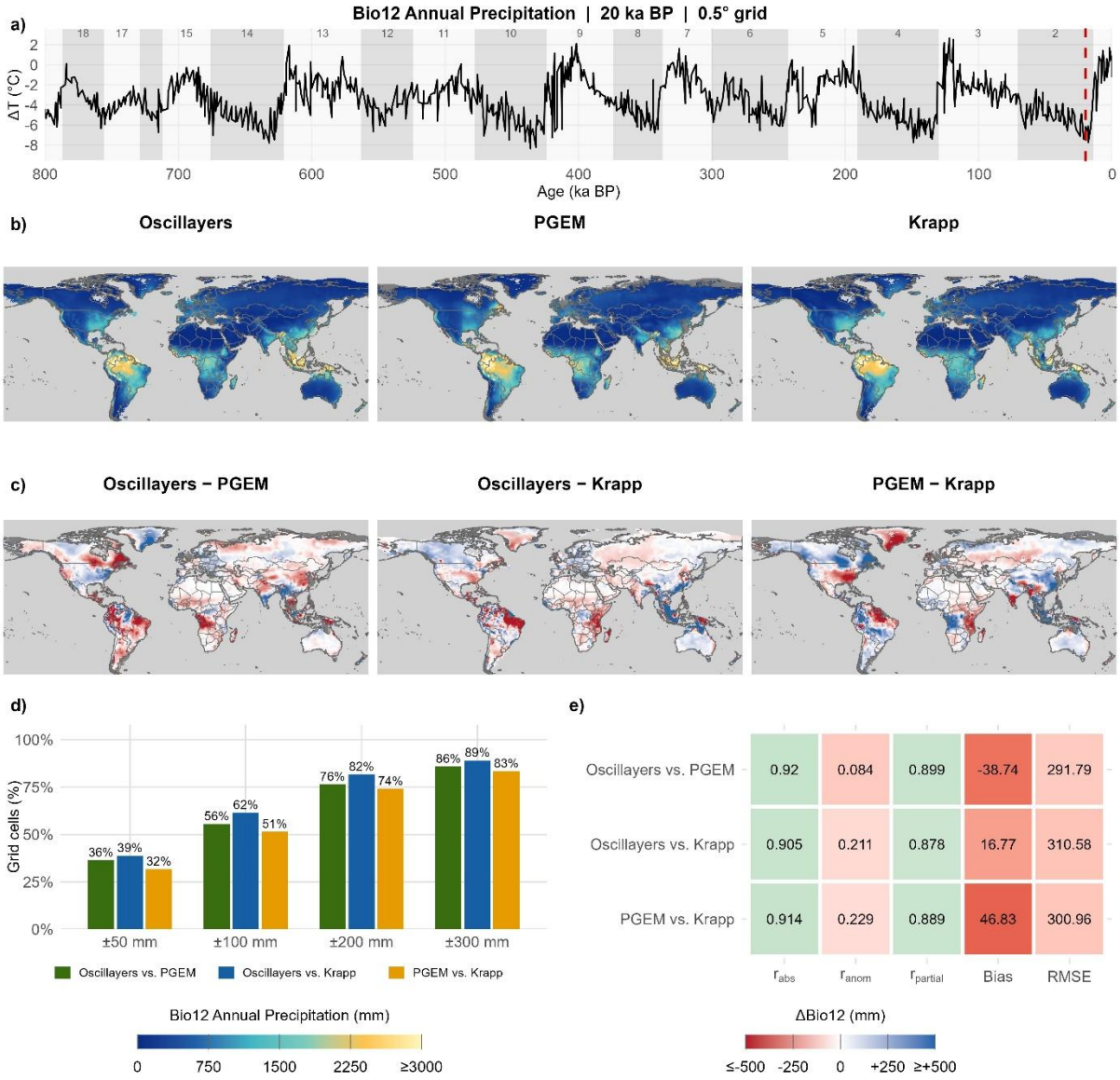

Figure 3. Comparison of total annual precipitation (BIO12) among the three paleoclimate reconstructions, Oscillayers, PGEM, and Krapp, at a single representative glacial time step (20 ka BP), on the common 0.5° grid using the Oscillayers land mask. (a) Global temperature anomaly curve of Hansen et al. (2013) across the last 800 kyr, with alternating shaded bands denoting Marine Isotope Stages (MIS 2–18, labelled); the red dashed line marks the time step shown. (b) Reconstructed BIO12 for each dataset. (c) Pairwise difference maps (Oscillayers − PGEM, Oscillayers − Krapp, PGEM − Krapp); red indicates that the first dataset is wetter, blue that it is drier. (d) Proportion of terrestrial grid cells for which the two datasets of each pair agree within ±50, ±100, ±200, and ±300 mm yr^{-1}. (e) Summary of pairwise agreement metrics for this time step: raw-value spatial correlation (r_{abs}), anomaly correlation (r_{anom}), latitude-partial correlation ($r_{partial}$), mean bias (mm yr^{-1}), and RMSE (mm yr^{-1}); cell

shading indicates the degree of agreement (green = stronger, red = weaker). As in Figure 2, the metrics in (e) refer to this single time step and differ from the multi-step means reported in the main text and Table 2. In contrast to temperature, the broad geography of wet and dry regions is reproduced consistently (high r_{abs}), whereas anomaly correlations are close to zero and the difference maps reveal extensive, spatially incoherent disagreement throughout the humid tropics, most pronounced across Amazonia, the Congo Basin, and South and Southeast Asia, demonstrating that even at the Last Glacial Maximum the reconstructions diverge substantially on regional precipitation. Sequences of all 79 time steps are provided in the Supplement (Additional File 2; see also Dryad repository (doi: https://doi.org/10.5061/dryad.qrfj6q5z8)).

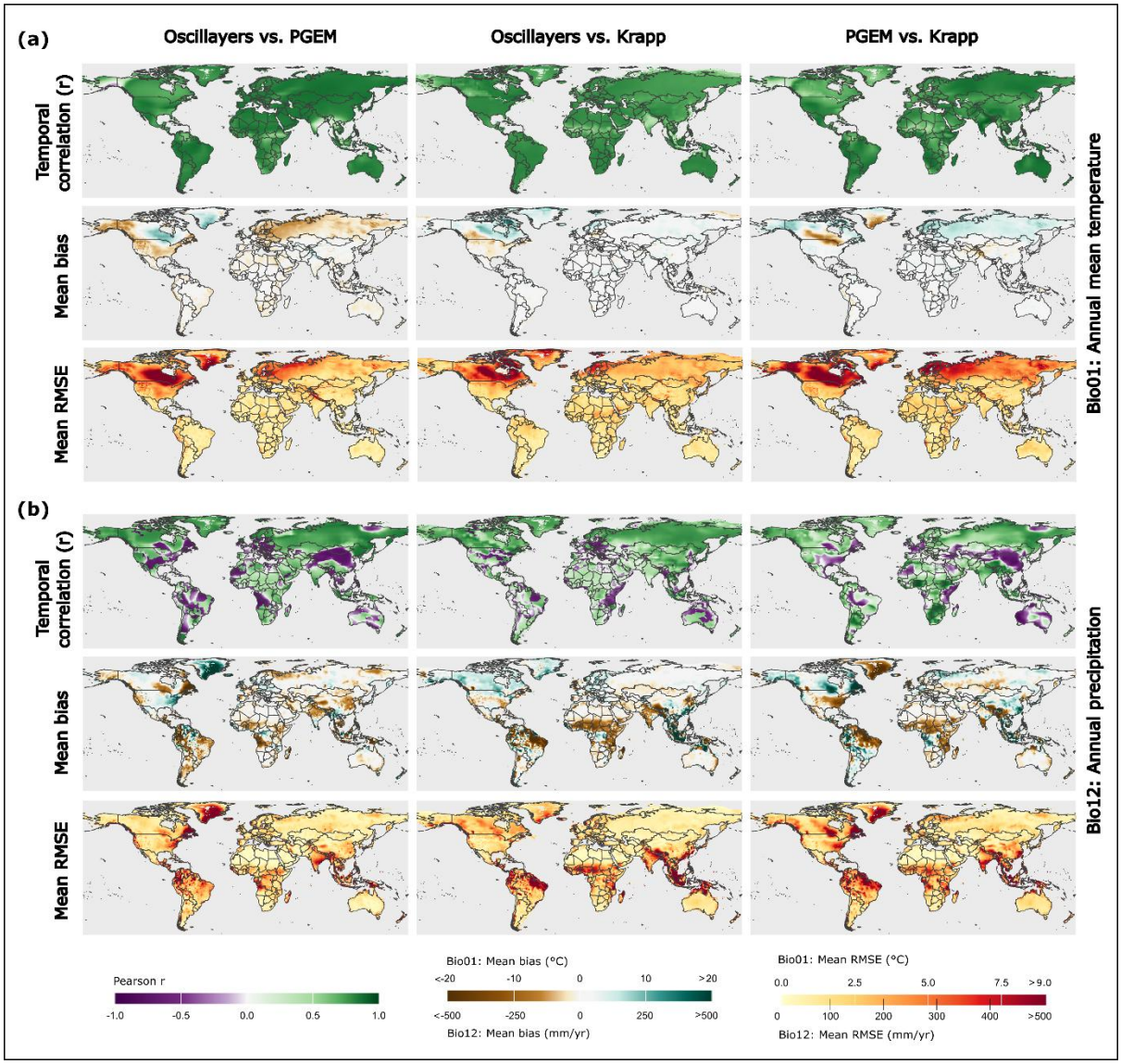

Figure 4. Cell-wise spatial maps of temporal agreement metrics for annual mean temperature (BIO1; panel a) and total annual precipitation (BIO12; panel b), computed across all 79 time slices (20–800 ka BP) for three dataset pairs. Rows show, from top to bottom: cell-wise Pearson correlation of the 79-step time series (r_{ts}), mean bias (DS1 − DS2), and mean RMSE. All metrics are aggregated over the full 800 ka record per grid cell. Positive bias values indicate that DS1 is warmer or wetter than DS2. Colour scales are shared across dataset pairs within each variable: Pearson r ranges from −1 to +1 (purple–white–green); mean bias is shown on a diverging scale centred at zero (brown–white–teal); mean RMSE uses a sequential scale from zero to the upper limit (yellow–red), with values exceeding the colour bar maximum (>9 °C for BIO1, >500 mm for BIO12) shown in the darkest shade.

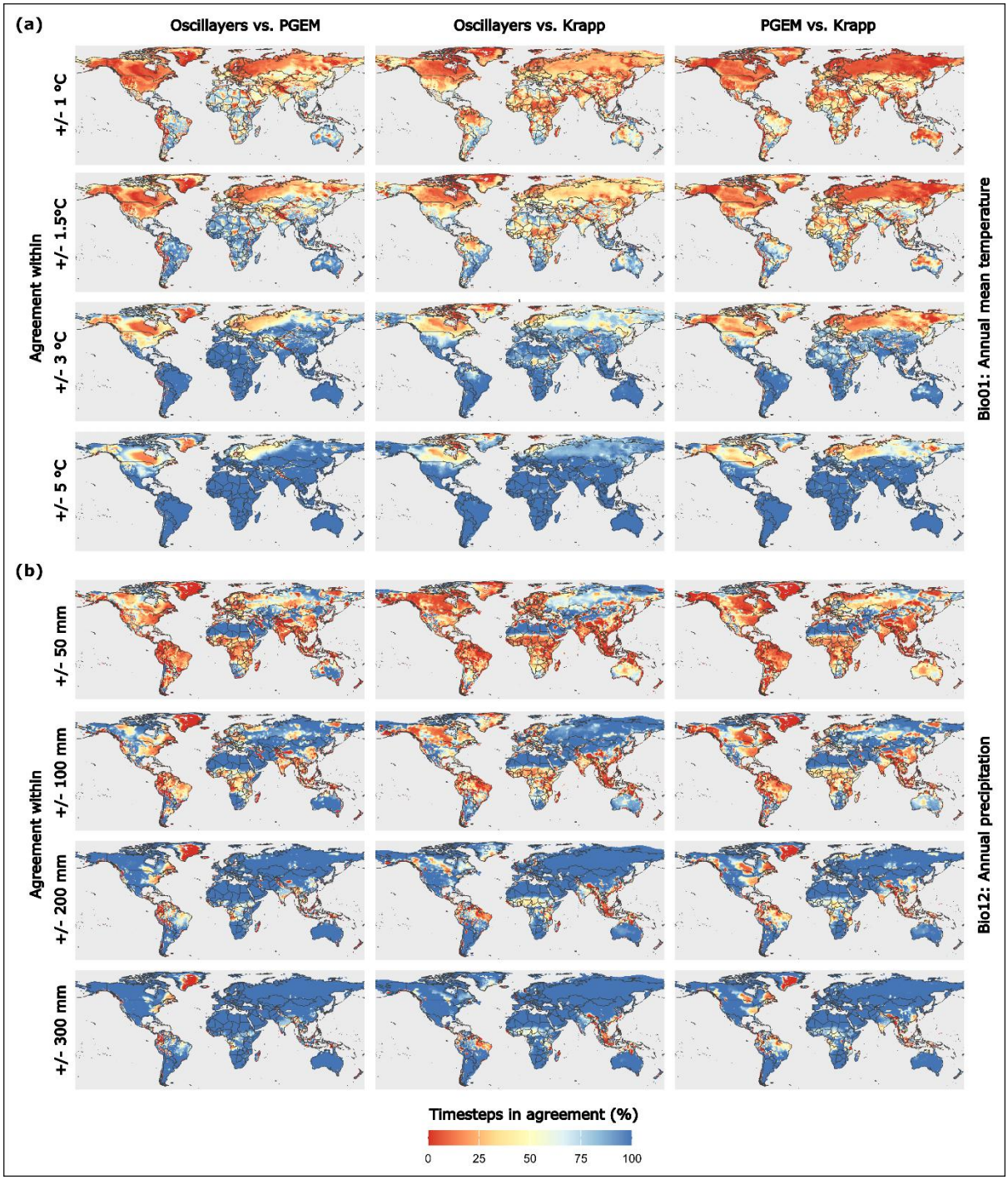

730

731 **Figure 5.** Cell-wise temporal agreement rates for annual mean temperature (BIO1; panel a) and total
732 annual precipitation (BIO12; panel b), shown for three dataset pairs and four agreement thresholds.
733 Colours indicate the percentage of the 79 time slices (20–800 ka BP) for which the absolute difference
734 between two reconstructions fell within the specified threshold at each grid cell (red: low agreement;
735 blue: high agreement). Thresholds for BIO1 are ±1 °C, ±1.5 °C, ±3 °C, and ±5 °C; thresholds for BIO12
736 are ±50 mm, ±100 mm, ±200 mm, and ±300 mm.

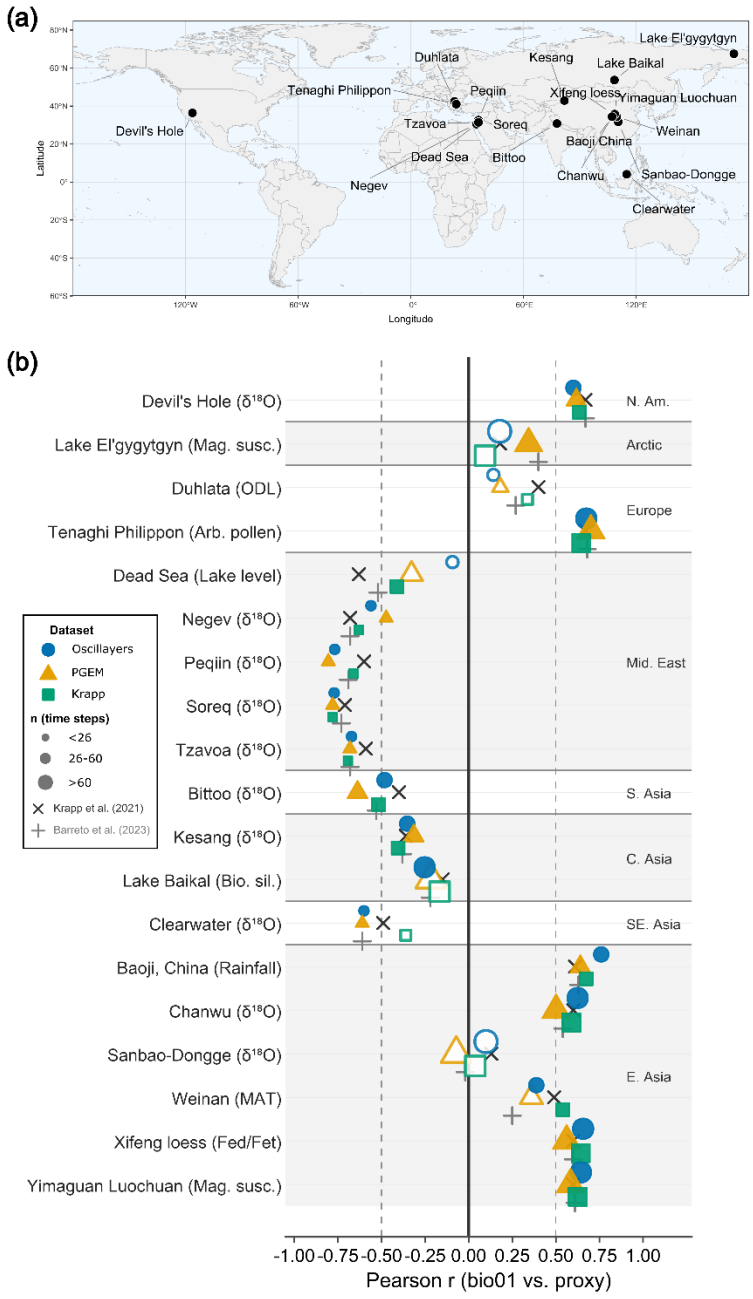

737

738 **Figure 6.** Proxy validation of BIO1 reconstructions against 19 terrestrial paleoclimate archives. (a)
739 Geographic distribution of proxy sites (as compiled by Krapp et al. 2021). (b) Pearson correlation
740 coefficients between each reconstruction and the corresponding proxy time series at each site, grouped
741 by region. Symbol shape and colour indicate the dataset (blue circles: Oscillayers; orange triangles:
742 PGEM; green squares: Krapp); symbol size reflects the number of overlapping time steps; open symbols
743 indicate sites where the correlation is not statistically significant ($p \geq 0.05$). Reference values from
744 Krapp et al. (2021; ×) and Barreto et al. (2023; +) are shown for comparison. Dashed vertical lines mark
745 $r = \pm 0.50$. Proxy archives are grouped by region (N. Am.: North America; Mid. East: Middle East; S.

Asia: South Asia; C. Asia: Central Asia; SE. Asia: Southeast Asia; E. Asia: East Asia). Proxy type is indicated in parentheses after each site name ($\delta^{18}O$: stable oxygen isotopes; Mag. susc.: magnetic susceptibility; ODL: organic dust layer; Arb. pollen: arboreal pollen; Bio. sil.: biogenic silica; MAT: mean annual temperature estimate; Fed/Fet: pedogenic iron ratio; Rainfall: rainfall reconstruction).

Supplement

Temperature converges, precipitation diverges: a systematic evaluation of three Quaternary paleoclimate reconstructions over the last 800,000 years

Supplemental Figure

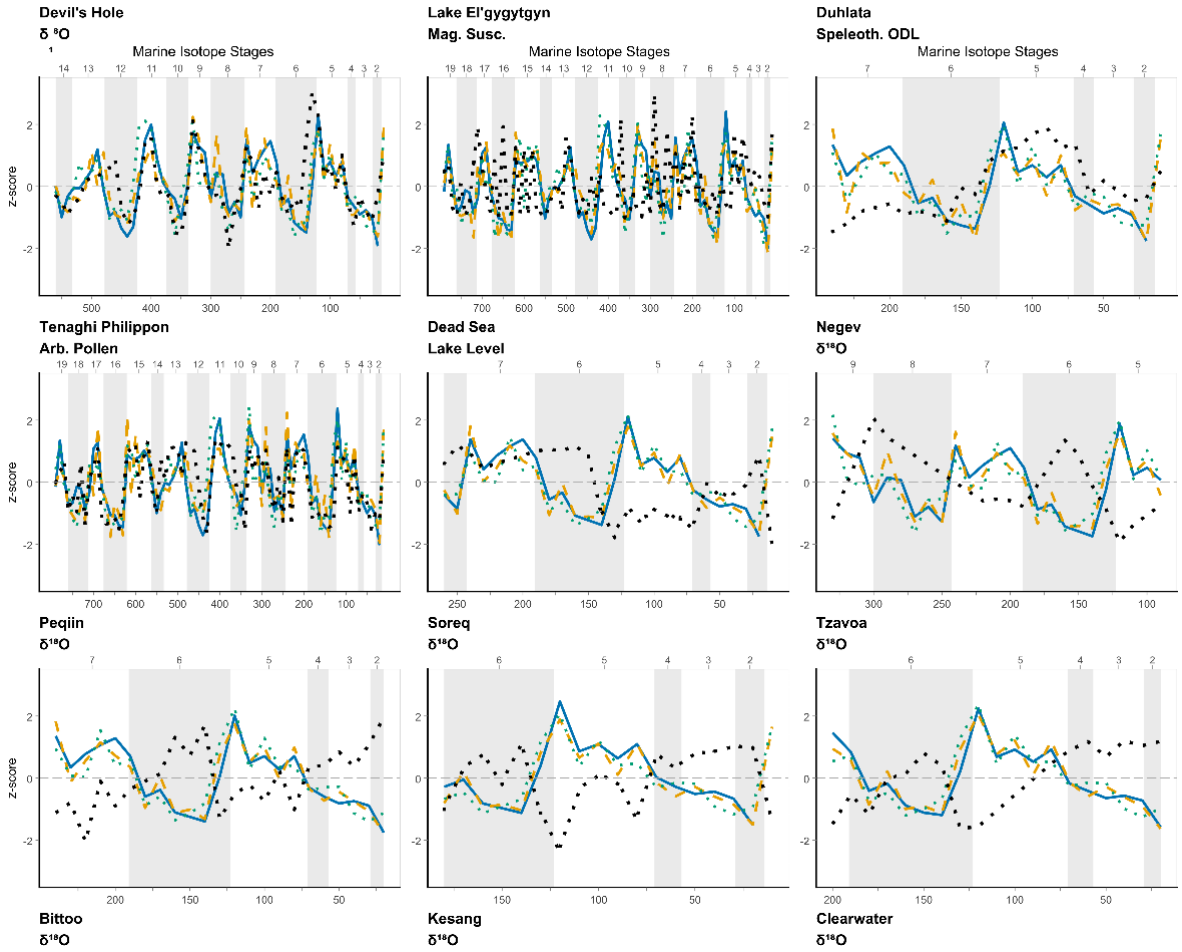

Supplemental Figure S1. Site-level comparison of BIO1 reconstructions and proxy time series across 19 terrestrial palaeoclimate archives. Each panel shows z-score standardised time series for Oscillayers (blue, solid), PGEM (orange, dashed), and Krapp (green, dotted) alongside the corresponding proxy record (black, dotted), plotted against age (ka BP). Marine Isotope Stages are indicated by alternating grey shading (odd stages: white; even stages: grey) with stage numbers shown along the upper axis. Site name and proxy type are given above each panel. All time series were z-score standardised prior to plotting to facilitate visual comparison across proxy types with different units and value ranges. See also the following page.

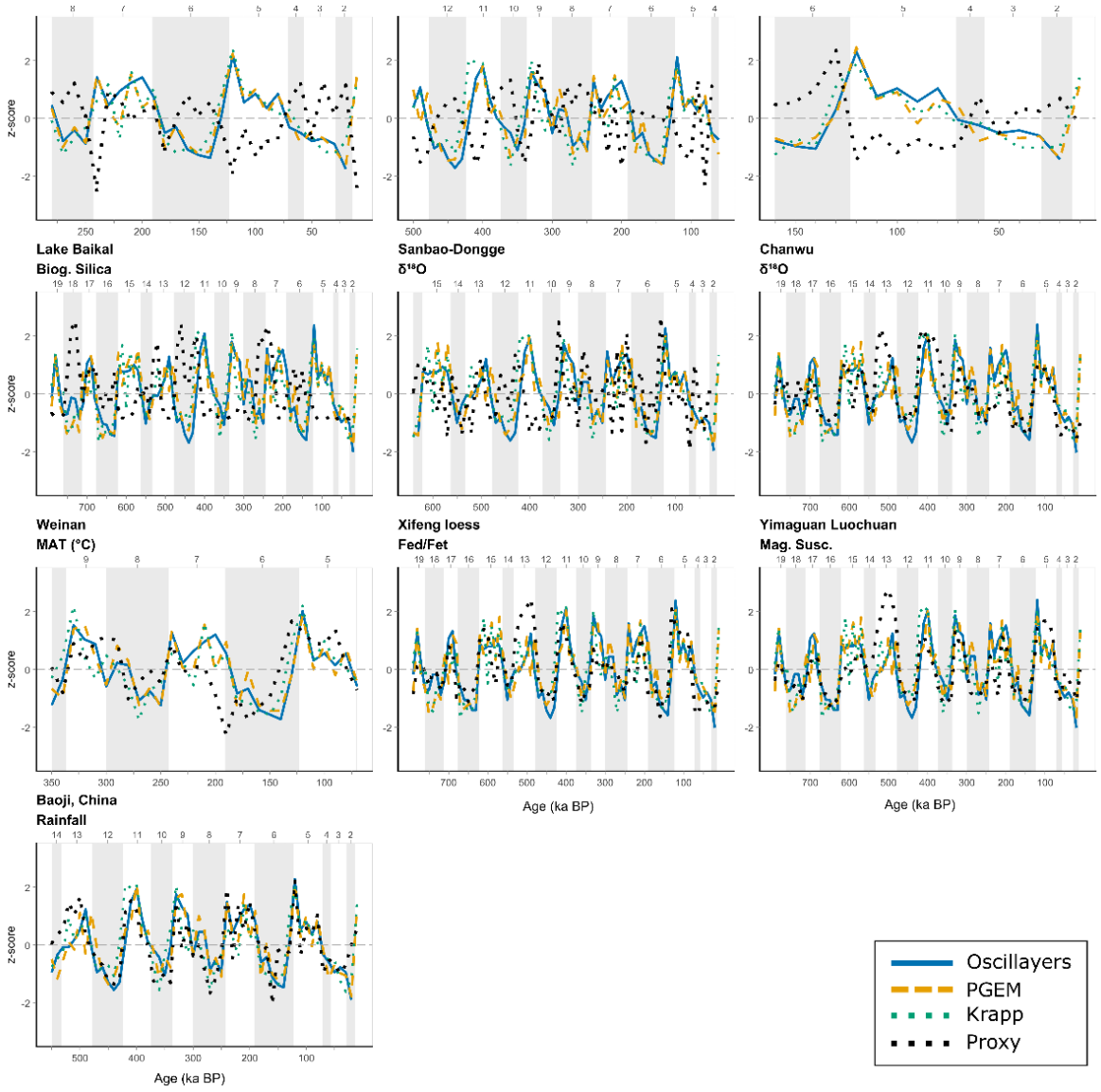

Supplemental Figure S1. Continued.